PoS(ICRC2025)442

Constraints on the spread of nuclear masses in ultra-high-energy cosmic rays based on the Phase I hybrid data from the Pierre Auger Observatory

Alexey Yushkov[a,*] **for the Pierre Auger Collaboration**[b]

[a]*Institute of Physics of the Czech Academy of Sciences, Na Slovance 1999/2, Prague, Czech Republic*

[b]*Observatorio Pierre Auger, Av. San Martín Norte 304, 5613 Malargüe, Argentina*
Full author list: https://www.auger.org/archive/authors_icrc_2025.html

E-mail: spokespersons@auger.org

We present an analysis of the correlation between the depth of the maximum of air-shower profiles and the signal in water-Cherenkov stations in events registered simultaneously by the fluorescence and surface detectors of the Pierre Auger Observatory. The analysis enables us to place constraints on the spread of nuclear masses in ultra-high-energy cosmic rays with a minor impact from the experimental systematic uncertainties and uncertainties in air-shower simulations. Due to this unique feature, the correlation analysis has previously allowed us to exclude all pure and proton-helium compositions near the ankle in the cosmic-ray energy spectrum at 5σ confidence level. The same property makes the correlation analysis an effective tool for testing the consistency of predictions of the post-LHC hadronic interaction models, including their latest versions such as EPOS LHC-R, QGSJet-III-01, Sibyll★ and Sibyll 2.3e. In this work, the correlation analysis using the Phase I hybrid data from the Pierre Auger Observatory is presented. The analysis uses the newest generation of hadronic interaction models and covers an extended energy range around the ankle in the cosmic-ray spectrum.

39th International Cosmic Ray Conference (ICRC2025)
15 – 24 July, 2025
Geneva, Switzerland

ICRC 2025
The Astroparticle Physics Conference
Geneva July 15-24, 2025

---

[*]Speaker

Introduction

Determining the mass composition is a key effort in understanding the origin of ultra-high-energy cosmic rays (UHECRs). The interpretation of air-shower data in terms of the absolute values of primary masses requires a comparison to predictions based on hadronic interaction models, imposing related systematic uncertainties. However, the correlation between the depth of the maximum of air-shower profiles, X_{max}, and number of muons at the ground has been shown to provide information about the spread of masses in the cosmic-ray beam with a minor dependence on the hadronic models [1]. Using the signal in water-Cherenkov detectors (WCDs) at 1000 meters from the shower core as a proxy for the muon number, the Pierre Auger Observatory [2] has demonstrated that pure compositions, as well as all mixes consisting only of two neighboring mass groups (proton-helium, helium-CNO, CNO-iron) are excluded for energies near the ankle in the energy spectrum [3]. In this work, we present a preliminary update of this analysis using the Phase I dataset of the Pierre Auger Observatory and the latest versions of post-LHC hadronic interaction models. Taking advantage of the minor dependence of the constraints on the spread of primary masses on details of hadronic interactions, we test the predictions of the post-LHC models by analyzing the energy and zenith-angle dependencies of the observed correlation.

1. The dataset and simulations

The analysis is performed using events that were successfully reconstructed with the Fluorescence Detector (FD) and Surface Detector (SD) of the Pierre Auger Observatory during the period (12/2004 − 12/2021). The FD event selection is the same as in the X_{max} analysis [4], except for the fiducial field of view selection. This cut is designed to minimize the selection bias (such as the loss of deep vertical events with X_{max} close to the ground) on the X_{max} distributions and does not affect the quality of individual events. In the correlation analysis, such bias is found to be minimal, particularly because events with zenith angles below 35°, corresponding to an atmospheric depth of $1060\,\mathrm{g\,cm^{-2}}$ at the location of the Observatory, are excluded. The justification from the point of view of the correlation analysis for selecting 35° as the minimum zenith angle is provided in Section 3.

To ensure an accurate estimation of the SD signal at 1000 meters from the core, it is required that the WCD with the highest signal in an event is surrounded by a hexagon with at least five active stations. The maximum zenith angle is limited to 60° to guarantee reliable SD reconstruction [5].

After selection, in the energy range $\lg(E/\mathrm{eV}) \in [18.3, 19.5]$ used in this work, the dataset consists of 9661 events. For the energy range $\lg(E/\mathrm{eV}) \in [18.5, 19.0]$ discussed in our previous publication [3], approximately 2.8 times more data is available in the current analysis.

The air-shower simulation library [6] for proton, helium, oxygen and iron primary species has been produced using CORSIKA 7.8010 [7]. The Auger $\overline{\text{Off}}\underline{\text{line}}$ framework [6, 8] has been used for the detector simulation and event reconstruction. For the analysis presented here, the newest versions of the post-LHC hadronic interaction models, namely EPOS LHC-R [9], QGSJet-III-01 [10, 11], Sibyll* [12], and Sibyll 2.3e [13], have been utilized. For more information about these models and their predictions regarding X_{max} and the muon shower content, see [14].

2. Constraints on the spread of primary masses

The spread of masses in the primary beam is estimated using the correlation between X_{max} and the signal in the WCDs located 1000 meters from the core, $S(1000)$ [3]. To avoid a decorrelation due to the spreads of energies and zenith angles, we use X_{max} and $S(1000)$ scaled to a reference energy of 10 EeV, for details, refer to [3]. Additionally, $S(1000)$ is scaled to a zenith angle of 38° as described in [15]. The scaled variables are referred to as X_{max}^* and S_{38}^*. They represent the values of X_{max} and $S(1000)$ that would have been observed if the shower had arrived at a zenith angle of 38° and an energy of 10 EeV. The correlation between X_{max}^* and S_{38}^* is assessed using a rank correlation coefficient r_G proposed in [16]. Rank correlation coefficients are invariant to the absolute values of $S(1000)$ and X_{max}, and therefore remain unaffected by systematic uncertainties in the corresponding predictions of hadronic models.

The correlation analysis leverages the general characteristics of air-shower development, which manifest as a nearly model-independent separation between mass groups in the (X_{max}^*, S_{38}^*) plane, as well as in the nearly model-independent magnitude of the fluctuations of these two observables. In Fig. 1, simulated X_{max}^* and S_{38}^* distributions are presented for SIBYLL 2.3e proton and iron showers, alongside the corresponding distribution observed in the data within the $\lg(E/\text{eV}) \in [18.5, 18.6]$ energy range. The correlation is positive for pure beams but becomes increasingly negative as the mass spread increases, reaching maximum anticorrelation for an extreme mix of protons and iron nuclei in equal proportions. The correlation in the data is negative, with a value in the middle between pure beams and the extreme mix. The statistical uncertainty is estimated as $\Delta r_G \simeq 0.9/\sqrt{N}$ [3], where N is the number of events in the dataset. The systematic uncertainty is $\Delta r_G(\text{sys.}) = {}^{+0.01}_{-0.02}$ [3]. The larger negative error arises from a small decorrelation introduced by the long-term performance of the FD and SD, for which no correction has been applied to stay conservative.

The energy evolution of the observed correlation is presented in Fig. 2 along with predictions from simulations using SIBYLL 2.3e and EPOS LHC-R. Up to the ankle ($\lg(E/\text{eV}) \approx 18.7$) the observed correlation is negative and differs significantly from the correlation for the pure beams. Above the ankle, r_G approaches to the values for pure beams. These observations hold for all hadronic interaction models used in this study. Additionally, in this plot, the correlation expected for the mass composition obtained from the fraction fits of the X_{max} distributions (hereafter referred to as 'FD X_{max} mix') is presented [17, 18]. One can see that r_G for the FD X_{max} mix differs significantly from the observed correlation below the ankle for SIBYLL 2.3e (and other SIBYLL versions[1]), while for EPOS LHC-R the agreement is good.

To interpret these findings one needs to convert r_G to the spread of the masses, $\sigma(\ln A)$, using Fig. 3. Each simulated point in this plot corresponds to a mixture with different fractions of (p, He, O, Fe) nuclei, the relative fractions change in 0.05 steps (4 points for pure compositions are grouped at $\sigma(\ln A) = 0$). Colors of the points indicate $\langle \ln A \rangle$ of each mix. In the energy bin $\lg(E/\text{eV}) \in [18.5, 18.6]$, shown in this plot, the r_G value in the data is compatible with $\sigma(\ln A) \in [1.0, 1.7]$. The evolution of the spread of the masses for the energy range $\lg(E/\text{eV}) \in [18.3, 19.0]$, obtained using this approach, is presented in Fig. 4. Independently of the hadronic interaction model used, in the energy range $\lg(E/\text{eV}) \in [18.3, 18.7]$, the spread of the masses remains within $\sigma(\ln A) \in [1.0, 1.7]$ interval. At higher energies, the limits on the mixing become

---

[1]We use the mix obtained with SIBYLL 2.3D which has the same X_{max} scale as that of SIBYLL 2.3e and SIBYLL★.
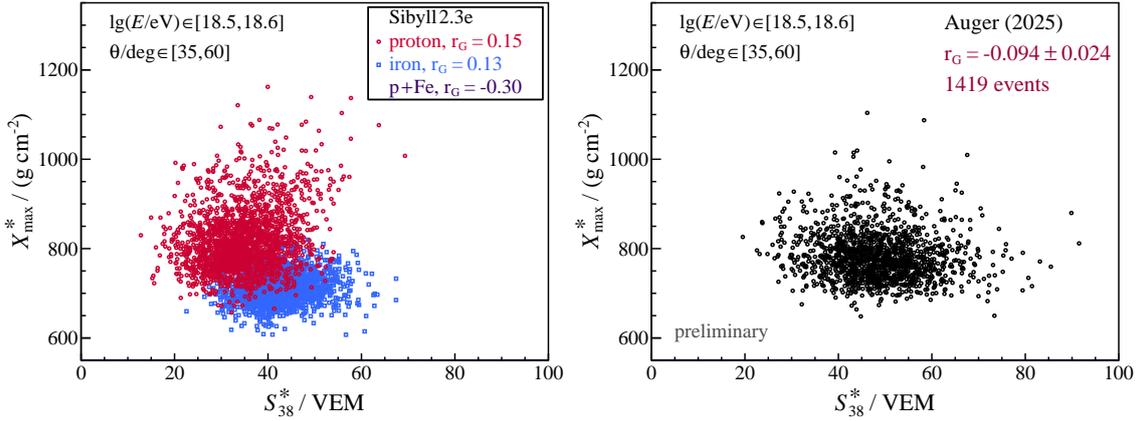
Figure 1: Correlation between X_{max}^* and S_{38}^*. Left panel: proton and iron showers (samples of 2000 events each) simulated with Sɪʙʏʟʟ 2.3e; the legend contains r_G values for pure beams and proton-iron equal mix (maximum mixing degree). Right panel: correlation in the data. Energy range: $\lg(E/\text{eV}) \in [18.5, 18.6]$; zenith angle range: $\theta/\text{deg} \in [35, 60]$.
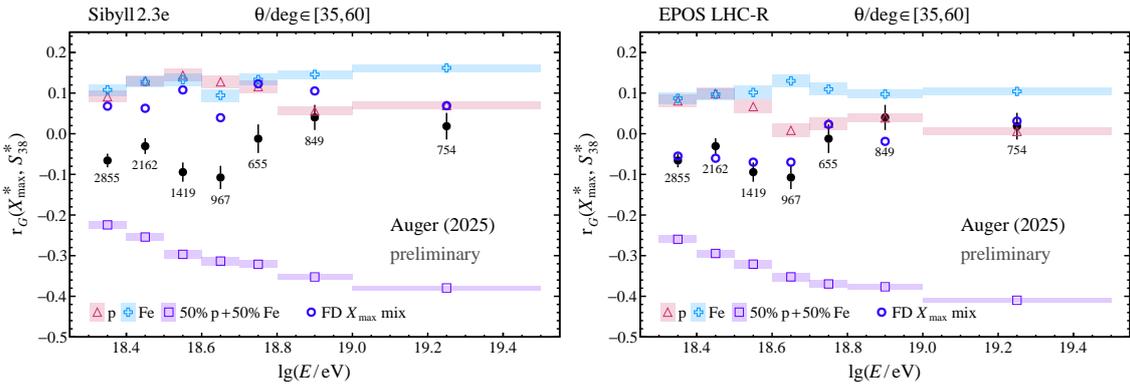

Figure 2: Energy dependence of the correlation in the data compared with correlations in simulations with Sɪʙʏʟʟ 2.3e and EPOS LHC-R for protons, iron nuclei and proton-iron equal mix. Additionally, the correlation expected for the mass composition inferred from fits of the FD X_{max} distributions [17, 18] is shown.

$\sigma(\ln A) \in [0.0, 1.3]$ (also for $\lg(E/\text{eV}) \in [19.0, 19.5]$, not shown here). These conclusions are valid for previous and even pre-LHC versions of the considered hadronic interaction models [3].

In Fig. 2, the discrepancy with the observed correlation below the ankle for Sɪʙʏʟʟ 2.3e can be explained by the proton-helium dominated FD X_{max} mix with typically $< 15\%$ contribution of nitrogen and $\sigma(\ln A) \in [0.8, 1.0]$. For EPOS LHC-R, instead, the FD X_{max} mix is dominated by protons and nitrogen (helium fraction is at maximum $\sim 20\%$) resulting in a larger mixing degree of $\sigma(\ln A) \in [1.2, 1.4]$ compatible with the constraints from the r_G analysis. Let us note that, in the forthcoming publication, the statistical and systematic uncertainties associated with the FD X_{max} mix fractions will be propagated to the r_G values to properly quantify these observations.
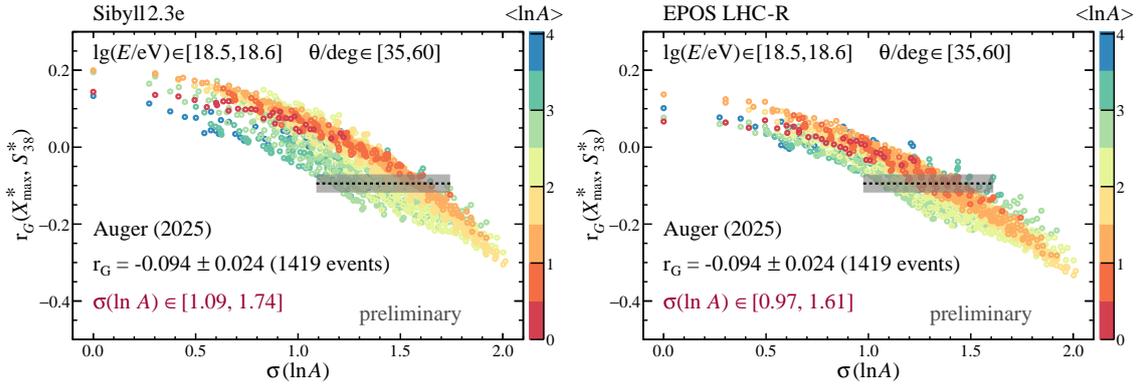
Figure 3: Conversion from r_G to $\sigma(\ln A)$ using simulations with SIBYLL 2.3e (left) and EPOS LHC-R (right). The shaded area represents the observed value with its statistical errors. The $\sigma(\ln A)$ ranges of the simulated mixes compatible with the correlation in the data are shown in each panel. See text for more details.
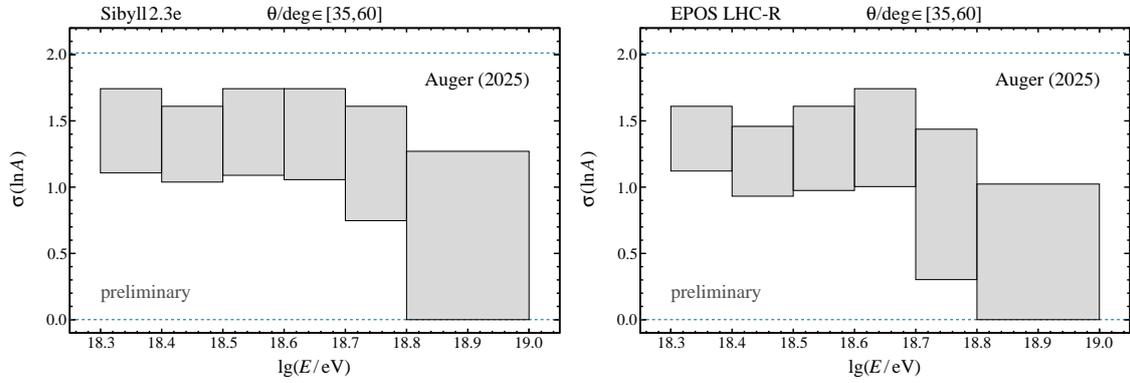

Figure 4: Constraints on $\sigma(\ln A)$ from the correlation analysis as a function of energy using SIBYLL 2.3e and EPOS LHC-R. Dashed lines indicate the values for pure compositions and the proton-iron equal mix (maximum mixing degree).
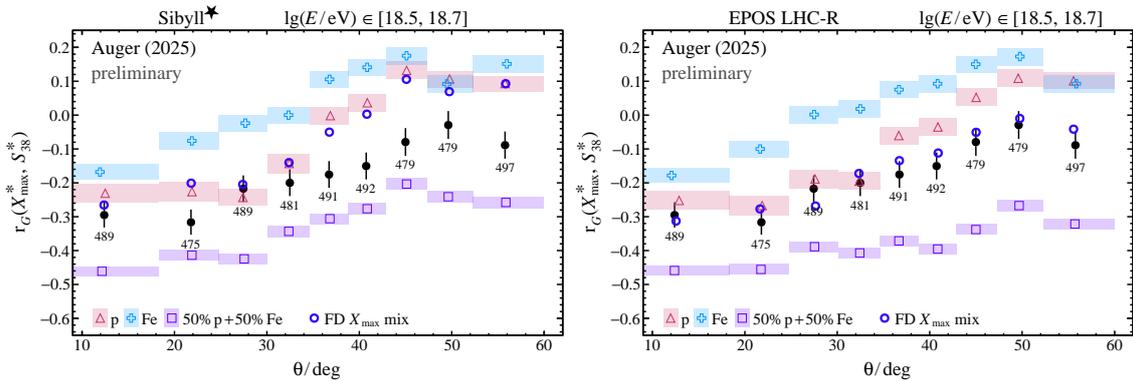
Figure 5: Zenith-angle dependence of r_G. The r_G values in the data are compared with SIBYLL* (left) and EPOS LHC-R (right) simulations for protons, iron nuclei, proton-iron equal mix, and the FD $X_{\max}$ mix. Energy range: $\lg(E/\text{eV}) \in [18.5, 18.7]$.

3. Zenith-angle dependence of the correlation

In Fig. 5, the zenith-angle dependence of the observed correlation for the energy range $\lg(E/\text{eV}) \in [18.5, 18.7]$ is compared with the hadronic interaction model predictions for (proton, iron, proton-iron equal mix) compositions and FD $X_{\max}$ mixes for SIBYLL* and EPOS LHC-R. These hadronic interaction models represent the extreme (currently existing) cases with the maximum muon content and the deepest $X_{\max}$ scale respectively. However, the qualitative behavior of $r_G(\theta)$ is similar across all other models. Regarding simulations, the r_G values for pure beams, particularly protons, remain significantly negative up to a zenith angle of $35°$. This anticorrelation does not become stronger even for relatively large degrees of mixing, as evidenced by the similarity of the correlations for pure protons, the FD $X_{\max}$ mix, and the data. As a consequence, the difference between r_G for pure protons and the extreme mix is approximately two times smaller than for zenith angles above $35°$. Exclusion of the events below $35°$ also improves the $\sigma(\ln A)$ constraints by reducing the width of the simulated distributions shown in Fig. 3, as it makes the r_G values for pure beams more similar to one another.

For zenith angles above $35°$, the discrepancies between the correlations in the data and those for the FD $X_{\max}$ mix are evident in the case of SIBYLL*. This demonstrates that the $\sim 30\%$ ad-hoc increase in the muon shower content in this model had no substantial impact on the simulated correlation values, and r_G for the FD $X_{\max}$ mix remained incompatible with the observed correlation, as was the case for SIBYLL 2.3e (c.f. Fig. 2).

In contrast, for EPOS LHC-R, its deeper $X_{\max}$ scale results in a larger spread of masses in the FD $X_{\max}$ mix, leading to a correlation similar to that observed in the data. Similar conclusions were obtained in [19], where a good description of the observed $S(1000)$ and $X_{\max}$ distributions was achieved by increasing the hadronic signal and shifting $X_{\max}$ to deeper values in earlier versions of the hadronic interaction models used here. The shift of the $X_{\max}$ scale in [19] led to inferences with a larger spread of masses and an improved description of the zenith-angle dependence of the correlation.

4. Summary

In this work, we have established constraints nearly independent of hadronic interaction models on the spread of the UHECR masses using the correlation between $X_{\max}$ and $S(1000)$ for events with energies $\lg(E/\text{eV}) \in [18.3, 19.5]$. For energies below the ankle in the UHECR spectrum, where we find $\sigma(\ln A) \in [1.0, 1.7]$, the mixes consisting only of the neighboring mass groups (p-He, He-CNO, CNO-Fe) are excluded. For higher energies, the mixing degree decreases to $\sigma(\ln A) \in [0.0, 1.3]$. These conclusions hold for any hadronic interaction model, including their pre-LHC versions, despite the fact that differences between models in muon shower content exceed the differences between proton and iron, and the differences in $X_{\max}$ scale amount to about half the proton-iron distance.

By analyzing the energy and zenith-angle dependences of the observed correlation for energies below the ankle, we established that the mass compositions obtained from the fits of the FD $X_{\max}$ distributions are not compatible with the correlation in the data for all interaction models, except for EPOS LHC-R. The deeper $X_{\max}$ scale in EPOS LHC-R, compared with other hadronic interaction

models, results in FD $X_{\max}$ mixes with the spread of the masses $\sigma(\ln A) \in [1.2, 1.4]$, with the energy and zenith-angle dependencies of the correlation agreeing with the observed ones. Similar results were obtained in our analysis [19], which employed previous versions of the hadronic interaction models with their $X_{\max}$ scales shifted to deeper values, resembling the $X_{\max}$ scale of EPOS LHC-R. Therefore, to match the observed correlation, adjusting the $X_{\max}$ scale must result in a stronger mass mixing in the compositions inferred from the $X_{\max}$ data. In addition, to achieve the same outcome, modifications to the $X_{\max}$ fluctuations or the proton-iron difference in $\langle X_{\max} \rangle$ could be considered.

A more detailed examination of the implications of the correlation analysis for the UHECR mass composition and the validation of the hadronic interaction model predictions will be reported in our forthcoming publication.

References

[1] P. Younk and M. Risse, *Sensitivity of the correlation between the depth of shower maximum and the muon shower size to the cosmic ray composition*, *Astropart.Phys.* **35** (2012) 807 [1203.3732].

[2] Pierre Auger Collaboration, *The Pierre Auger Cosmic Ray Observatory*, *Nucl. Instrum. Meth.* **A798** (2015) 172 [1502.01323].

[3] Pierre Auger Collaboration, *Evidence for a mixed mass composition at the 'ankle' in the cosmic-ray spectrum*, *Phys. Lett.* **B762** (2016) 288 [1609.08567].

[4] T. Fitoussi, *Depth of maximum of air-shower profiles above $10^{17.8}$ eV measured with the fluorescence detector of the Pierre Auger Observatory and mass-composition implications*, *PoS* **ICRC2023** (2023) 319.

[5] Pierre Auger Collaboration, *Reconstruction of events recorded with the surface detector of the Pierre Auger Observatory*, *JINST* **15** (2020) P10021 [2007.09035].

[6] E. Santos, *Update on the Offline Framework for AugerPrime and production of reference simulation libraries using the VO Auger grid resources*, *PoS* **ICRC2023** (2023) 248.

[7] D. Heck et al., *CORSIKA: A Monte Carlo code to simulate extensive air showers*, Report FZKA-6019 (1998).

[8] Pierre Auger Collaboration, *The Offline Software Framework of the Pierre Auger Observatory*, *Nucl. Instrum. Methods Phys. Res.* **580** (2007) 1485.

[9] T. Pierog and K. Werner, *EPOS LHC-R : up-to-date hadronic model for EAS simulations*, *PoS* **ICRC2023** (2023) 230.

[10] S. Ostapchenko, *QGSJET-III model of high energy hadronic interactions: The formalism*, *Phys. Rev. D* **109** (2024) 034002.

[11] S. Ostapchenko, *QGSJET-III model of high energy hadronic interactions. II. Particle production and extensive air shower characteristics*, *Phys. Rev. D* **109** (2024) 094019.

[12] F. Riehn, R. Engel and A. Fedynitch, *Sibyll* ★*: ad-hoc modifications for an improved description of muon data in extensive air showers*, *PoS* **ICRC2023** (2023) 429 [2309.05390].

[13] F. Riehn et al., *Hadronic interaction model Sibyll 2.3d and extensive air showers*, *Phys. Rev. D* **102** (2020) 063002 [1912.03300].

[14] T. Pierog, *EPOS LHC-R: A Global Approach to Solve the Muon Puzzle*, Presented at FZU – Institute of Physics of the Czech Academy of Sciences (2025), https://indico.fzu.cz/event/303/.

[15] Pierre Auger Collaboration, *Measurement of the cosmic-ray energy spectrum above* 2.5×10^{18} *eV using the Pierre Auger Observatory*, *Phys. Rev. D* **102** (2020) 062005 [2008.06486].

[16] R. Gideon and R. Hollister, *A rank correlation coefficient resistant to outliers*, *Journal of the American Statistical Association* **82** (1987) 656.

[17] O. Tkachenko, *Studies of the mass composition of cosmic rays and proton-proton interaction cross-sections at ultra-high energies with the Pierre Auger Observatory*, *PoS* **ICRC2023** (2023) 438.

[18] O. Tkachenko, *Measurement of the Inelastic Proton-Proton Cross Section at* $\sqrt{s} \geq 40$ *TeV using the Hybrid Data of the Pierre Auger Observatory*, these proceedings.

[19] Pierre Auger Collaboration, *Testing hadronic-model predictions of depth of maximum of air-shower profiles and ground-particle signals using hybrid data of the Pierre Auger Observatory*, *Phys. Rev. D* **109** (2024) 102001 [2401.10740].

The Pierre Auger Collaboration

A. Abdul Halim[13], P. Abreu[70], M. Aglietta[53,51], I. Allekotte[1], K. Almeida Cheminant[78,77], A. Almela[7,12], R. Aloisio[44,45], J. Alvarez-Muñiz[76], A. Ambrosone[44], J. Ammerman Yebra[76], G.A. Anastasi[57,46], L. Anchordoqui[83], B. Andrada[7], L. Andrade Dourado[44,45], S. Andringa[70], L. Apollonio[58,48], C. Aramo[49], E. Arnone[62,51], J.C. Arteaga Velázquez[66], P. Assis[70], G. Avila[11], E. Avocone[56,45], A. Bakalova[31], F. Barbato[44,45], A. Bartz Mocellin[82], J.A. Bellido[13], C. Berat[35], M.E. Bertaina[62,51], M. Bianciotto[62,51], P.L. Biermann[a], V. Binet[5], K. Bismark[38,7], T. Bister[77,78], J. Biteau[36,i], J. Blazek[31], J. Blümer[40], M. Boháčová[31], D. Boncioli[56,45], C. Bonifazi[8], L. Bonneau Arbeletche[22], N. Borodai[68], J. Brack[f], P.G. Brichetto Orchera[7,40], F.L. Briechle[41], A. Bueno[75], S. Buitink[15], M. Buscemi[46,57], M. Büsken[38,7], A. Bwembya[77,78], K.S. Caballero-Mora[65], S. Cabana-Freire[76], L. Caccianiga[58,48], F. Campuzano[6], J. Caraça-Valente[82], R. Caruso[57,46], A. Castellina[53,51], F. Catalani[19], G. Cataldi[47], L. Cazon[76], M. Cerda[10], B. Čermáková[40], A. Cermenati[44,45], J.A. Chinellato[22], J. Chudoba[31], L. Chytka[32], R.W. Clay[13], A.C. Cobos Cerutti[6], R. Colalillo[59,49], R. Conceição[70], G. Consolati[48,54], M. Conte[55,47], F. Convenga[44,45], D. Correia dos Santos[27], P.J. Costa[70], C.E. Covault[81], M. Cristinziani[43], C.S. Cruz Sanchez[3], S. Dasso[4,2], K. Daumiller[40], B.R. Dawson[13], R.M. de Almeida[27], E.-T. de Boone[43], B. de Errico[27], J. de Jesús[7], S.J. de Jong[77,78], J.R.T. de Mello Neto[27], I. De Mitri[44,45], J. de Oliveira[18], D. de Oliveira Franco[42], F. de Palma[55,47], V. de Souza[20], E. De Vito[55,47], A. Del Popolo[57,46], O. Deligny[33], N. Denner[31], L. Deval[53,51], A. di Matteo[51], C. Dobrigkeit[22], J.C. D'Olivo[67], L.M. Domingues Mendes[16,70], Q. Dorosti[43], J.C. dos Anjos[16], R.C. dos Anjos[26], J. Ebr[31], F. Ellwanger[40], R. Engel[38,40], I. Epicoco[55,47], M. Erdmann[41], A. Etchegoyen[7,12], C. Evoli[44,45], H. Falcke[77,79,78], G. Farrar[85], A.C. Fauth[22], T. Fehler[43], F. Feldbusch[39], A. Fernandes[70], M. Fernandez[14], B. Fick[84], J.M. Figueira[7], P. Filip[38,7], A. Filipčič[74,73], T. Fitoussi[40], B. Flaggs[87], T. Fodran[77], A. Franco[47], M. Freitas[70], T. Fujii[86,h], A. Fuster[7,12], C. Galea[77], B. García[6], C. Gaudu[37], P.L. Ghia[33], U. Giaccari[47], F. Gobbi[10], F. Gollan[7], G. Golup[1], M. Gómez Berisso[1], P.F. Gómez Vitale[11], J.P. Gongora[11], J.M. González[1], N. González[7], D. Góra[68], A. Gorgi[53,51], M. Gottowik[40], F. Guarino[59,49], G.P. Guedes[23], L. Gülzow[40], S. Hahn[38], P. Hamal[31], M.R. Hampel[7], P. Hansen[3], V.M. Harvey[13], A. Haungs[40], T. Hebbeker[41], C. Hojvat[d], J.R. Hörandel[77,78], P. Horvath[32], M. Hrabovský[32], T. Huege[40,15], A. Insolia[57,46], P.G. Isar[72], M. Ismaiel[77,78], P. Janecek[31], V. Jilek[31], K.-H. Kampert[37], B. Keilhauer[40], A. Khakurdikar[77], V.V. Kizakke Covilakam[7,40], H.O. Klages[40], M. Kleifges[39], J. Köhler[40], F. Krieger[41], M. Kubatova[31], N. Kunka[39], B.L. Lago[17], N. Langner[41], N. Leal[7], M.A. Leigui de Oliveira[25], Y. Lema-Capeans[76], A. Letessier-Selvon[34], I. Lhenry-Yvon[33], L. Lopes[70], J.P. Lundquist[73], M. Mallamaci[60,46], D. Mandat[31], P. Mantsch[d], F.M. Mariani[58,48], A.G. Mariazzi[3], I.C. Mariş[14], G. Marsella[60,46], D. Martello[55,47], S. Martinelli[40,7], M.A. Martins[76], H.-J. Mathes[40], J. Matthews[g], G. Matthiae[61,50], E. Mayotte[82], S. Mayotte[82], P.O. Mazur[d], G. Medina-Tanco[67], J. Meinert[37], D. Melo[7], A. Menshikov[39], C. Merx[40], S. Michal[31], M.I. Micheletti[5], L. Miramonti[58,48], M. Mogarkar[68], S. Mollerach[1], F. Montanet[35], L. Morejon[37], K. Mulrey[77,78], R. Mussa[51], W.M. Namasaka[37], S. Negi[31], L. Nellen[67], K. Nguyen[84], G. Nicora[9], M. Niechciol[43], D. Nitz[84], D. Nosek[30], A. Novikov[87], V. Novotny[30], L. Nožka[32], A. Nucita[55,47], L.A. Núñez[29], J. Ochoa[7,40], C. Oliveira[20], L. Östman[31], M. Palatka[31], J. Pallotta[9], S. Panja[31], G. Parente[76], T. Paulsen[37], J. Pawlowsky[37], M. Pech[31], J. Pękala[68], R. Pelayo[64], V. Pelgrims[14], L.A.S. Pereira[24], E.E. Pereira Martins[38,7], C. Pérez Bertolli[7,40], L. Perrone[55,47], S. Petrera[44,45], C. Petrucci[56], T. Pierog[40], M. Pimenta[70], M. Platino[7], B. Pont[77], M. Pourmohammad Shahvar[60,46], P. Privitera[86], C. Priyadarshi[68], M. Prouza[31], K. Pytel[69], S. Querchfeld[37], J. Rautenberg[37], D. Ravignani[7], J.V. Reginatto Akim[22], A. Reuzki[41], J. Ridky[31], F. Riehn[76,j], M. Risse[43], V. Rizi[56,45], E. Rodriguez[7,40], G. Rodriguez Fernandez[50], J. Rodriguez Rojo[11], S. Rossoni[42], M. Roth[40], E. Roulet[1], A.C. Rovero[4], A. Saftoiu[71], M. Saharan[77], F. Salamida[56,45], H. Salazar[63], G. Salina[50], P. Sampathkumar[40], N. San Martin[82], J.D. Sanabria Gomez[29], F. Sánchez[7], E.M. Santos[21], E. Santos[31], F. Sarazin[82], R. Sarmento[70], R. Sato[11], P. Savina[44,45], V. Scherini[55,47], H. Schieler[40], M. Schimassek[33], M. Schimp[37], D. Schmidt[40], O. Scholten[15,b], H. Schoorlemmer[77,78], P. Schovánek[31], F.G. Schröder[87,40], J. Schulte[41], T. Schulz[31], S.J. Sciutto[3], M. Scornavacche[7], A. Sedoski[7], A. Segreto[52,46], S. Sehgal[37], S.U. Shivashankara[73], G. Sigl[42], K. Simkova[15,14], F. Simon[39], R. Šmída[86], P. Sommers[e], R. Squartini[10], M. Stadelmaier[40,48,58], S. Stanič[73], J. Stasielak[68], P. Stassi[35], S. Strähnz[38], M. Straub[41], T. Suomijärvi[36], A.D. Supanitsky[7], Z. Svozilikova[31], K. Syrokvas[30], Z. Szadkowski[69], F. Tairli[13], M. Tambone[59,49], A. Tapia[28], C. Taricco[62,51], C. Timmermans[78,77], O. Tkachenko[31], P. Tobiska[31], C.J. Todero Peixoto[19], B. Tomé[70], A. Travaini[10], P. Travnicek[31], M. Tueros[3], M. Unger[40], R. Uzeiroska[37], L. Vaclavek[32], M. Vacula[32], I. Vaiman[44,45], J.F. Valdés Galicia[67], L. Valore[59,49], P. van Dillen[77,78], E. Varela[63], V. Vašíčková[37], A. Vásquez-Ramírez[29], D. Veberič[40], I.D. Vergara Quispe[3], S. Verpoest[87], V. Verzi[50], J. Vicha[31], J. Vink[80], S. Vorobiov[73], J.B. Vuta[31], C. Watanabe[27], A.A. Watson[c], A. Weindl[40], M. Weitz[37], L. Wiencke[82], H. Wilczyński[68], B. Wundheiler[7], B. Yue[37], A. Yushkov[31], E. Zas[76], D. Zavrtanik[73,74], M. Zavrtanik[74,73]

9

[1] Centro Atómico Bariloche and Instituto Balseiro (CNEA-UNCuyo-CONICET), San Carlos de Bariloche, Argentina

[2] Departamento de Física and Departamento de Ciencias de la Atmósfera y los Océanos, FCEyN, Universidad de Buenos Aires and CONICET, Buenos Aires, Argentina

[3] IFLP, Universidad Nacional de La Plata and CONICET, La Plata, Argentina

[4] Instituto de Astronomía y Física del Espacio (IAFE, CONICET-UBA), Buenos Aires, Argentina

[5] Instituto de Física de Rosario (IFIR) – CONICET/U.N.R. and Facultad de Ciencias Bioquímicas y Farmacéuticas U.N.R., Rosario, Argentina

[6] Instituto de Tecnologías en Detección y Astropartículas (CNEA, CONICET, UNSAM), and Universidad Tecnológica Nacional – Facultad Regional Mendoza (CONICET/CNEA), Mendoza, Argentina

[7] Instituto de Tecnologías en Detección y Astropartículas (CNEA, CONICET, UNSAM), Buenos Aires, Argentina

[8] International Center of Advanced Studies and Instituto de Ciencias Físicas, ECyT-UNSAM and CONICET, Campus Miguelete – San Martín, Buenos Aires, Argentina

[9] Laboratorio Atmósfera – Departamento de Investigaciones en Láseres y sus Aplicaciones – UNIDEF (CITEDEF-CONICET), Argentina

[10] Observatorio Pierre Auger, Malargüe, Argentina

[11] Observatorio Pierre Auger and Comisión Nacional de Energía Atómica, Malargüe, Argentina

[12] Universidad Tecnológica Nacional – Facultad Regional Buenos Aires, Buenos Aires, Argentina

[13] University of Adelaide, Adelaide, S.A., Australia

[14] Université Libre de Bruxelles (ULB), Brussels, Belgium

[15] Vrije Universiteit Brussels, Brussels, Belgium

[16] Centro Brasileiro de Pesquisas Fisicas, Rio de Janeiro, RJ, Brazil

[17] Centro Federal de Educação Tecnológica Celso Suckow da Fonseca, Petropolis, Brazil

[18] Instituto Federal de Educação, Ciência e Tecnologia do Rio de Janeiro (IFRJ), Brazil

[19] Universidade de São Paulo, Escola de Engenharia de Lorena, Lorena, SP, Brazil

[20] Universidade de São Paulo, Instituto de Física de São Carlos, São Carlos, SP, Brazil

[21] Universidade de São Paulo, Instituto de Física, São Paulo, SP, Brazil

[22] Universidade Estadual de Campinas (UNICAMP), IFGW, Campinas, SP, Brazil

[23] Universidade Estadual de Feira de Santana, Feira de Santana, Brazil

[24] Universidade Federal de Campina Grande, Centro de Ciencias e Tecnologia, Campina Grande, Brazil

[25] Universidade Federal do ABC, Santo André, SP, Brazil

[26] Universidade Federal do Paraná, Setor Palotina, Palotina, Brazil

[27] Universidade Federal do Rio de Janeiro, Instituto de Física, Rio de Janeiro, RJ, Brazil

[28] Universidad de Medellín, Medellín, Colombia

[29] Universidad Industrial de Santander, Bucaramanga, Colombia

[30] Charles University, Faculty of Mathematics and Physics, Institute of Particle and Nuclear Physics, Prague, Czech Republic

[31] Institute of Physics of the Czech Academy of Sciences, Prague, Czech Republic

[32] Palacky University, Olomouc, Czech Republic

[33] CNRS/IN2P3, IJCLab, Université Paris-Saclay, Orsay, France

[34] Laboratoire de Physique Nucléaire et de Hautes Energies (LPNHE), Sorbonne Université, Université de Paris, CNRS-IN2P3, Paris, France

[35] Univ. Grenoble Alpes, CNRS, Grenoble Institute of Engineering Univ. Grenoble Alpes, LPSC-IN2P3, 38000 Grenoble, France

[36] Université Paris-Saclay, CNRS/IN2P3, IJCLab, Orsay, France

[37] Bergische Universität Wuppertal, Department of Physics, Wuppertal, Germany

[38] Karlsruhe Institute of Technology (KIT), Institute for Experimental Particle Physics, Karlsruhe, Germany

[39] Karlsruhe Institute of Technology (KIT), Institut für Prozessdatenverarbeitung und Elektronik, Karlsruhe, Germany

[40] Karlsruhe Institute of Technology (KIT), Institute for Astroparticle Physics, Karlsruhe, Germany

[41] RWTH Aachen University, III. Physikalisches Institut A, Aachen, Germany

[42] Universität Hamburg, II. Institut für Theoretische Physik, Hamburg, Germany

[43] Universität Siegen, Department Physik – Experimentelle Teilchenphysik, Siegen, Germany

[44] Gran Sasso Science Institute, L'Aquila, Italy

[45] INFN Laboratori Nazionali del Gran Sasso, Assergi (L'Aquila), Italy

[46] INFN, Sezione di Catania, Catania, Italy

[47] INFN, Sezione di Lecce, Lecce, Italy

[48] INFN, Sezione di Milano, Milano, Italy

[49] INFN, Sezione di Napoli, Napoli, Italy

[50] INFN, Sezione di Roma "Tor Vergata", Roma, Italy

[51] INFN, Sezione di Torino, Torino, Italy

[52] Istituto di Astrofisica Spaziale e Fisica Cosmica di Palermo (INAF), Palermo, Italy

[53] Osservatorio Astrofisico di Torino (INAF), Torino, Italy

[54] Politecnico di Milano, Dipartimento di Scienze e Tecnologie Aerospaziali , Milano, Italy

[55] Università del Salento, Dipartimento di Matematica e Fisica "E. De Giorgi", Lecce, Italy

[56] Università dell'Aquila, Dipartimento di Scienze Fisiche e Chimiche, L'Aquila, Italy

[57] Università di Catania, Dipartimento di Fisica e Astronomia "Ettore Majorana", Catania, Italy

[58] Università di Milano, Dipartimento di Fisica, Milano, Italy

[59] Università di Napoli "Federico II", Dipartimento di Fisica "Ettore Pancini", Napoli, Italy

[60] Università di Palermo, Dipartimento di Fisica e Chimica "E. Segrè", Palermo, Italy

[61] Università di Roma "Tor Vergata", Dipartimento di Fisica, Roma, Italy

[62] Università Torino, Dipartimento di Fisica, Torino, Italy

[63] Benemérita Universidad Autónoma de Puebla, Puebla, México

[64] Unidad Profesional Interdisciplinaria en Ingeniería y Tecnologías Avanzadas del Instituto Politécnico Nacional (UPIITA-IPN), México, D.F., México

[65] Universidad Autónoma de Chiapas, Tuxtla Gutiérrez, Chiapas, México

[66] Universidad Michoacana de San Nicolás de Hidalgo, Morelia, Michoacán, México

[67] Universidad Nacional Autónoma de México, México, D.F., México

[68] Institute of Nuclear Physics PAN, Krakow, Poland

[69] University of Łódź, Faculty of High-Energy Astrophysics,Łódź, Poland

[70] Laboratório de Instrumentação e Física Experimental de Partículas – LIP and Instituto Superior Técnico – IST, Universidade de Lisboa – UL, Lisboa, Portugal

[71] "Horia Hulubei" National Institute for Physics and Nuclear Engineering, Bucharest-Magurele, Romania

[72] Institute of Space Science, Bucharest-Magurele, Romania

[73] Center for Astrophysics and Cosmology (CAC), University of Nova Gorica, Nova Gorica, Slovenia

[74] Experimental Particle Physics Department, J. Stefan Institute, Ljubljana, Slovenia

[75] Universidad de Granada and C.A.F.P.E., Granada, Spain

[76] Instituto Galego de Física de Altas Enerxías (IGFAE), Universidade de Santiago de Compostela, Santiago de Compostela, Spain

[77] IMAPP, Radboud University Nijmegen, Nijmegen, The Netherlands

[78] Nationaal Instituut voor Kernfysica en Hoge Energie Fysica (NIKHEF), Science Park, Amsterdam, The Netherlands

[79] Stichting Astronomisch Onderzoek in Nederland (ASTRON), Dwingeloo, The Netherlands

[80] Universiteit van Amsterdam, Faculty of Science, Amsterdam, The Netherlands

[81] Case Western Reserve University, Cleveland, OH, USA

[82] Colorado School of Mines, Golden, CO, USA

[83] Department of Physics and Astronomy, Lehman College, City University of New York, Bronx, NY, USA

[84] Michigan Technological University, Houghton, MI, USA

[85] New York University, New York, NY, USA

[86] University of Chicago, Enrico Fermi Institute, Chicago, IL, USA

[87] University of Delaware, Department of Physics and Astronomy, Bartol Research Institute, Newark, DE, USA

——

[a] Max-Planck-Institut für Radioastronomie, Bonn, Germany

[b] also at Kapteyn Institute, University of Groningen, Groningen, The Netherlands

[c] School of Physics and Astronomy, University of Leeds, Leeds, United Kingdom

[d] Fermi National Accelerator Laboratory, Fermilab, Batavia, IL, USA

[e] Pennsylvania State University, University Park, PA, USA

[f] Colorado State University, Fort Collins, CO, USA

[g] Louisiana State University, Baton Rouge, LA, USA

[h] now at Graduate School of Science, Osaka Metropolitan University, Osaka, Japan

[i] Institut universitaire de France (IUF), France

[j] now at Technische Universität Dortmund and Ruhr-Universität Bochum, Dortmund and Bochum, Germany

Acknowledgments

PoS(ICRC2025)442